J. Biochem. **135**, 525–532 (2004)
DOI: 10.1093/jb/mvh061

Mutational Effects on O^6-Methylguanine-DNA Methyltransferase from Hyperthermophile: Contribution of Ion-Pair Network to Protein Thermostability

Shingo Nishikori[1], Kentaro Shiraki[1], Kiyonobu Yokota[1], Naoshige Izumikawa[1], Shinsuke Fujiwara[2], Hiroshi Hashimoto[3], Tadayuki Imanaka[4] and Masahiro Takagi[*,1]

[1]School of Materials Science, Japan Advanced Institute for Science and Technology, 1-1 Asahidai, Tatsunokuchi, Ishikawa 923-1292; [2]Department of Bioscience, School of Science and Technology, Kwansei-Gakuin University, 2-1 Gakuen Sanda, Hyogo 669-1337; [3]Science of Biological Supermolecular Systems, Graduate School of Integrated Science, Yokohama City University, Suehiro-cho, Tsurumi-ku, Yokohama, Kanagawa 230-0045; and [4]Department of Synthetic Chemistry and Biological Chemistry, Graduate School of Engineering, Kyoto University, Katsura, Nishikyo-ku, Kyoto 615-8510

Received January 27, 2004; accepted February 20, 2004

Ion pairs have been considered to be general stabilizing factors in hyperthermophilic proteins, but the present experimental data cannot fully explain how ion pairs and ion-pair networks contribute to the stability. In this paper, we show experimental evidence that not all of the internal ion pairs contribute to the thermal and thermodynamic stability, using O^6-methylguanine-DNA methyltransferase from *Thermococcus kodakaraensis* KOD1 (*Tk*-MGMT) as a model protein. Of three mutants in which an inter-helical ion pair was disrupted, only one mutant (E93A) was shown to be destabilized. ΔG of E93A was lower by ~4 kJ mol^{-1} than that of the wild type, and E93A unfolded one order of magnitude faster than did the wild type and other variants. Glu 93 has unique properties in forming an ion-pair network that bridges the N- and C-terminal domains and connects three helices in the protein interior.

Key words: Archaea, ion-pair network, hyperthermostable protein, thermodynamics, thermal stability.

Abbreviations: AdaC, C-terminal fragment of the Ada protein; CD, circular dichroism; GdnHCl, guanidine hydrochloride; IPTG, isopropyl-thio-β-D-galactopyranoside; MGMT, O^6-methylguanine-DNA methyltransferase; PDB, protein databank; *Tk, Thermococcus kodakaraensis*; Tris, tris(hydroxymethyl)aminomethane; SDS-PAGE, sodium dodecyl sulfate polyacrylamide gel electrophoresis.

Electrostatic interaction is proposed as a universally important factor affecting the thermal stability of hyperthermophilic proteins. A comparison of the tertiary structures of several proteins derived from hyperthermophiles with those of their mesophilic counterparts showed that the hyperthermophilic proteins contain an increased number of ion pairs (which often tend to be organized in large networks). For example, glutamate dehydrogenase from *Pyrococcus furiosus* (*Pf*-GDH) possesses more ion pairs and larger ion-pair networks than its mesophilic counterpart from *Clostridium symbiosum* (*1*). Such structural studies on hyperthermophilic proteins were followed by studies of rubredoxin from *Pyrococcus furiosus* (*2*), glyceraldehyde-3-phosphate dehydrogenase (GAPDH) from *Thermotoga maritima* (*3*), indole-3-glycerol phosphate synthase from *Sulfolobus solfataricus* (*4*) and iron-superoxide dismutase from *Aquifex pyrophilus* (*5*). These structural data imply that an increased number of ion pairs and their networks play a crucial role in the thermal stability of hyperthermophilic proteins.

On the other hand, estimates of the energy contribution of an ion pair to protein stability have led to conflicting conclusions, ranging from stabilizing (*6–11*), through insignificant (*12–14*), to destabilizing (*15–17*). It is widely accepted that solvent accessibility is the one of the most important criteria for determining the energetic stabilization of ion pairs, due to differences in the dielectric constant (*18*): *i.e.*, it is quite plausible that surface ion pairs contribute little to protein stability, while buried ion pairs stabilize the native structure due to a microheterogeneity in low dielectric conditions. However, case reports of individual proteins indicate that the contribution of ion pairs in the interior of a protein is sensitive to conformational variability. Our understanding of the role of ion pairs in stabilizing native structures has recently become very ambiguous.

We have investigated O^6-methylguanine-DNA methyltransferase derived from the hyperthermophilic archaeon *Thermococcus kodakaraensis* strain KOD1 (*Tk*-MGMT, EC 2.1.1.63) as a model protein. *Tk*-MGMT is one of the most thermostable proteins, with a melting temperature of 108°C, which is 50°C higher than its mesophilic counterpart protein (AdaC) from *Escherichia coli* (*19*). It is a monomer with a relative molecular mass of 19.5 kDa (174 amino acids), and its high resolution X-ray crystal structure has been solved (Fig. 1) (*20*). *Tk*-MGMT contains no cofactors necessary for folding, such as disulfide bridges or *cis*-proline, and it shows full reversibility from its chemically unfolded condition (*19*).

[*]To whom correspondence should be addressed. Tel: +81-761-51-1650, Fax: +81-761-51-1655, E-mail: takagi@jaist.ac.jp

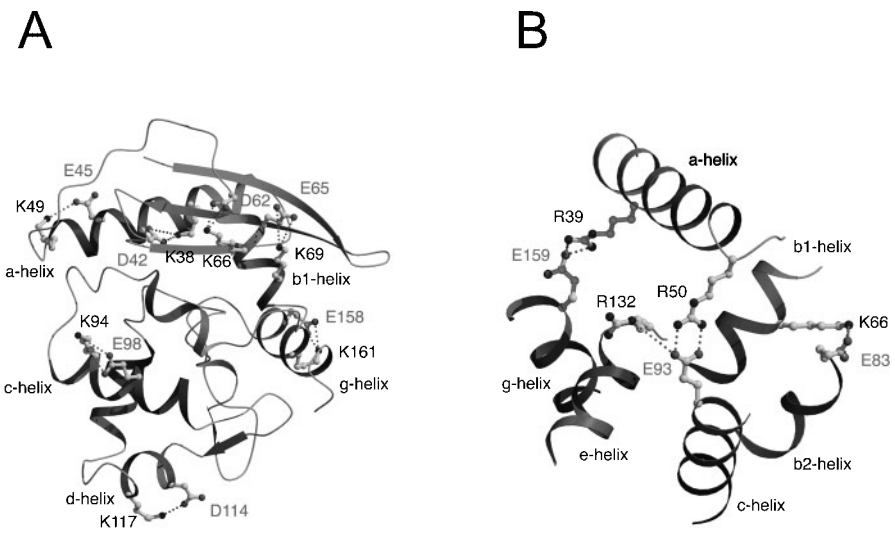

Fig. 1. **Ribbon models of *Tk*-MGMT.** (A) All intra-helical ion pairs are shown by a ball-and-stick model. (B) Three buried and inter-helical ion pairs, Lys 66-Glu 83, Arg 50-Glu 93-Arg 132, and Lys 39-Glu 159, are shown by a ball-and-stick model.

Tk-MGMT has seven intra-helical ion pairs, as judged by distances of within 5 Å between the side-chains of Arg, Asp, Glu, and Lys, while AdaC has none. Figure 1A shows the intra-helical ion pairs in *Tk*-MGMT. A model experiment has shown that the intra-helical ion pairs contribute to reinforce the stability of the helical conformation (*21*). Furthermore, *Tk*-MGMT has six inter-helical ion pairs, while AdaC has only two. These two ion pairs in AdaC (His 147–Glu 173 and Arg 148–Glu 173) are structurally conserved in *Tk*-MGMT (His 142–Glu 167 and Arg 143–Glu 167). Figure 1B shows the extra four helical ion pairs in *Tk*-MGMT. Arg 39–Glu 159 connects the a- and g-helices over a short distance (2.83 Å for NH1-OE2 and 3.02 Å for NH2-OE2), while Arg 50–Glu 93 connects the a- and c-helices over the shortest distance (2.74 Å for NH1-OE1 and 2.83 Å for NH2-OE2). This ion pair also forms an ion-pair network with Arg 132 on the e-helix. This ion pair and the ion-pair network connect the N- and the C-terminal domains. Lys 66–Glu 83 in *Tk*-MGMT forms an ion pair with a separation of 3.39 Å for NH-OE1 and of 3.95 Å for NH-OE2 in the N-terminal domain between the b1- and b2-helices (Fig. 1B). Lys 66 also forms an intra-helical ion pair with Asp 62 in the b1-helix (Fig. 1A). In this study, we constructed four mutants by disrupting the intra- and inter-helical ion pairs, and investigated their stability thermodynamically and kinetically. We show new data whereby the thermodynamic and kinetic contributions of the ion pair are not explained solely by solvent accessibility, but also by other factors such as network formation across the helices.

MATERIAL AND METHODS

Site-Directed Mutagenesis—Site-directed mutagenesis was performed using the following primers for the various *Tk*-MGMT mutants.

E83A-5: 5′-GCCAGCTTTCTCCGGGCACTTTCCTTTGAGGGC-3′.

E83A-3: 5′-GCCCTCAAAGGAAAGTGCCCGGAGAAAGCTGGC-3′.

E93A-5: 5′-TCCTTTGAGGGCGTTACACCCTTTGCGAAGAAGGTTTAC-3′.

E93A-3: 5′-TGTGAGCCACTCGTAAACCTTCTTCGCAAAGGGTGTAAC-3′.

E158A-5: 5′-ATTGTTTACTACAGCTCCGGGATTGCGGAAAAGAAGTTC-3′.

E158A-3: 5′-AATTTCCAGCAGGAACTTCTTTTCCGCAATCCCGGAGCT-3′.

E159A-5: 5′-AGCTCCGGGATTGAGGCAAAGAAGTTCCTGCTG-3′.

E159A-3: 5′-CAGCAGGAACTTCTTTGCCTCAATCCCGGAGCT-3′.

All mutants were constructed by PCR, using a *Tk*-mgmt gene in plasmid pET-8c (*22*). The constructed mutant genes were confirmed by DNA sequencing.

Expression and Purification of Tk-MGMT Variants—Recombinant variants were expressed by IPTG induction in HMS174 (DE3) pLysS cells and purified to homogeneity as described previously (*22*). The homogeneity of the purified protein was confirmed by SDS-PAGE. Protein concentrations were determined using a molar absorption coefficient of 18,000 M^{-1} cm^{-1} at 280 nm (*23*).

Equilibrium Studies—The GdnHCl-induced titration curves for the wild type and the mutants were obtained by measuring CD signals at 222 nm of equilibrated samples containing various concentrations of GdnHCl. Complete unfolding of *Tk*-MGMT was accomplished by incubating the enzymes at 37°C for 1 day in the presence of 7.2 M GdnHCl. For renaturation transitions, unfolded enzymes were mixed with buffer solutions (50 mM TrisHCl, pH 8.0) containing the desired concentrations of GdnHCl. The samples were incubated at 37°C for 3 days to achieve complete equilibrium. Final protein concentration was adjusted to 0.1 mg/ml.

The experimental data were analyzed by a two-state folding mechanism. Briefly, the apparent equilibrium constant (K_{app}) was determined by using Eq. 1,

$$K_{app} = f_U/f_N = (y_N - y)/(y - y_U) \quad (1)$$

where f_N and f_U are the fractions of folded and unfolded states, and y_N, y_U, and y represent the signals of the folded, unfolded, and monitored intensity, respectively. The free-energy change (ΔG) of the equilibrium measurement is related to the apparent equilibrium constant by

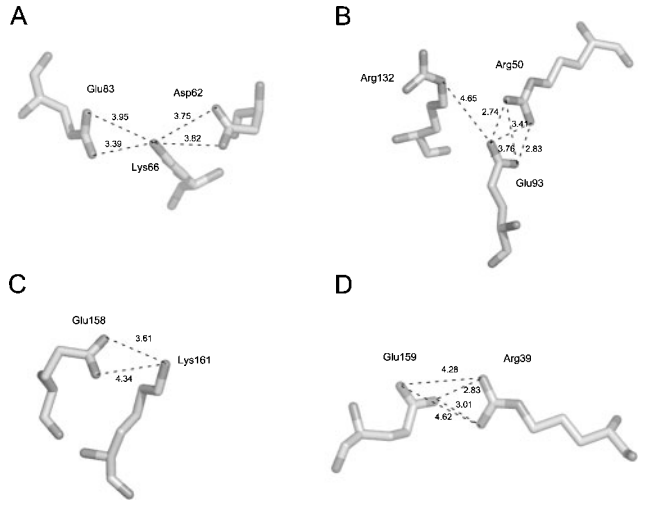

Fig. 2. **The structure in the vicinity of the mutation sites at (A) Glu 83, (B) Glu 93, (C) Glu 158, and (D) Glu 159.**

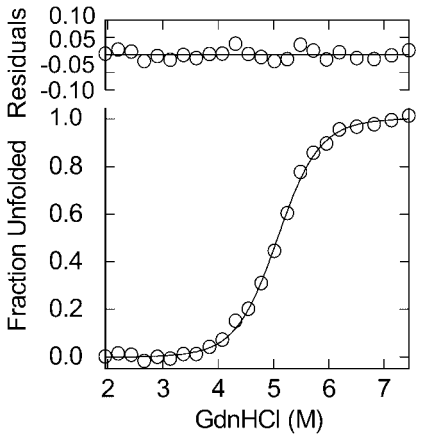

Fig. 3. **Representative data of GdnHCl-induced titration curve of the wild type monitored by CD at 222 nm at 20°C.** Solid lines show the result of the nonlinear regression analysis according to Eq. 1.

$\Delta G = -RT \ln K_{app}$, where R is the gas constant. A two-state unfolding model assumes a linear dependence between free energy and the denaturant concentration as Eq. 2,

$$\Delta G_{Gdn} = \Delta G_{H2O} - m\ [\text{GdnHCl}] \quad (2)$$

where m represents the dependence of ΔG_{Gdn} on denaturant concentration. In order to obtain the temperature dependence of ΔG_{H2O}, the GdnHCl-induced unfolding profiles of *Tk*-MGMT variants were obtained at 10, 20, 30, 40, 50, 60, and 70°C.

ΔG_{H2O} and m were calculated by curve-fitting to the observed ellipticity change using a calculation program (Igor Pro, WaveMatrics, Oregon, USA). Generally, the value of ΔG_{H2O} is very sensitive to small errors in m value, due to the long extrapolation to 0 M GdnHCl concentration, while the denaturation at 50% unfolding ($[\text{GdnHCl}]_{50\%}$) is very reproducible (*13*, *24*). For the precise determination of $\Delta\Delta G$ (the difference of free-energy change between the wild type and the mutants), Eq. 3 was used,

$$\Delta\Delta G = \langle m \rangle \times ([\text{GdnHCl}]_{wt50\%} - [\text{GdnHCl}]_{mut50\%}) \quad (3)$$

where $\langle m \rangle$ is the average value of the slopes for *Tk*-MGMT variants, and $[\text{GdnHCl}]_{wt50\%}$ and $[\text{GdnHCl}]_{mut50\%}$ correspond to the mid-points for the denaturant concentrations on the titration curves for wild type and the mutant, respectively.

Kinetic Studies—The unfolding kinetics of *Tk*-MGMT variants were monitored at 50°C by CD at 222 nm, using manual mixing, with a 1 cm pathlength cuvette. Unfolding experiments were carried out by a 1:9 dilution of folded *Tk*-MGMT (2 mg/ml of protein, 200 mM TrisHCl, pH 8.0) resulting in unfolding conditions of 7.2 M GdnHCl, 20 mM TrisHCl (pH 8.0). The kinetic data for unfolding were fitted by a non-linear least-squares method with following Eq. 4,

$$A(t) = A_0 + A_1 \Sigma\ \alpha_i \exp(-k_i t) \quad (4)$$

where $A(t)$, A_0, and A_1 are the observed amplitude at time t, the amplitude at dead-end time, and the total amplitude, respectively; k_i is the rate constant at the i-th kinetic phase; and α_i is the fractional amplitude at the i-th kinetic phase.

Thermal Unfolding of Tk-MGMT Variants in 5 M Urea—Thermal unfolding curves were measured by continuously measuring the ellipticity at 222 nm between 40 and 99°C at a scan rate of 18°C h^{-1} and with data collection every 0.1°C.

Energy Minimization for Tk-MGMT Variants—To estimate the structure of *Tk*-MGMT variants, an energy minimization program was utilized based on the X-ray crystal structure of wild-type *Tk*-MGMT (*20*). The coordinates for the *Tk*-MGMT variants were taken from PDB file code 1mgt. The appropriate residues were changed at the site of the mutation, and all hydrogens were explicitly treated in the protein models. Energy minimization of *Tk*-MGMT was conducted with the InsightII program (Accelrys, San Diego, CA) with the force field Discover CVFF (consistent valence force field). The structure of *Tk*-MGMT variants was subjected to energy minimization calculations in vacuum by the steepest descent method with 10,000 iterations. The root-mean-square deviation (RMSD) of estimated structures between the wild type and mutants was calculated. The radius of the solvent probe was 1.4 Å.

RESULTS

Design of Mutant Enzymes—Tk-MGMT has seven intrahelical ion pairs on the protein surface, and four inter-helical ion pairs in the protein interior in addition to the two ion pairs conserved in AdaC. To evaluate the contribution of the internal ion pairs to protein stability, we focused on three residues, Glu 83, Glu 93 and Glu 159. These residues are in the protein interior and have solvent-accessible surface areas (SASAs) of 16.7% (Glu 83), 7.2% (Glu 93), and 8.2% (Glu 159). Glu 93 is located at the center of the ion-pair network of Arg 50–Glu 93–Arg 132. Glu83 forms an ion-pair network with Lys 66 and Asp 62. As a surface ion pair, we focused on the most solvent-accessi-

Table 1. **Temperature dependent free-energy change between the wild type and E83A, E93A, E158A, and E159A.**[a]

Temperature	Protein	m[b] (kJ mol^{-1} M^{-1})	[GdnHCl]$_{50\%}$[c] (M)	$\Delta\Delta G$[d] (kJ mol^{-1})
10°C	wild type	7.38 ± 0.43	5.14 ± 0.02	
	E83A	8.65 ± 1.21	4.99 ± 0.44	–1.17
	E93A	7.08 ± 0.43	4.58 ± 0.02	–4.06
	E158A	6.11 ± 0.44	5.15 ± 0.03	0.09
	E159A	5.85 ± 0.21	5.02 ± 0.02	–0.72
20°C	wild type	7.89 ± 0.47	5.15 ± 0.02	
	E83A	9.61 ± 1.40	5.00 ± 0.04	–1.36
	E93A	7.54 ± 0.46	4.63 ± 0.02	–4.04
	E158A	6.39 ± 0.47	5.16 ± 0.03	0.04
	E159A	6.45 ± 0.26	5.05 ± 0.02	–0.72
30°C	wild type	8.14 ± 0.48	5.15 ± 0.02	
	E83A	9.78 ± 1.32	5.00 ± 0.04	–1.34
	E93A	8.06 ± 0.48	4.64 ± 0.02	–4.19
	E158A	6.79 ± 0.48	5.16 ± 0.02	0.07
	E159A	6.86 ± 0.31	5.06 ± 0.02	–0.70
40°C	wild type	8.06 ± 0.51	5.14 ± 0.02	
	E83A	9.62 ± 1.20	4.97 ± 0.03	–1.50
	E93A	8.07 ± 0.47	4.57 ± 0.02	–4.56
	E158A	6.92 ± 0.49	5.14 ± 0.03	0.04
	E159A	6.73 ± 0.30	5.03 ± 0.02	–0.75
50°C	wild type	6.53 ± 0.44	4.98 ± 0.03	
	E83A	8.20 ± 0.87	4.78 ± 0.04	–1.48
	E93A	8.74 ± 0.50	4.37 ± 0.02	–4.65
	E158A	6.09 ± 0.48	4.99 ± 0.04	0.03
	E159A	6.09 ± 0.31	4.90 ± 0.03	–0.54
60°C	wild type	7.30 ± 0.41	4.51 ± 0.02	
	E83A	9.01 ± 0.74	4.32 ± 0.04	–1.52
	E93A	8.50 ± 0.44	4.06 ± 0.02	–3.58
	E158A	6.96 ± 0.58	4.54 ± 0.04	0.18
	E159A	6.52 ± 0.28	4.51 ± 0.02	0.02
70°C	wild type	6.63 ± 0.49	3.88 ± 0.03	
	E83A	9.78 ± 1.09	3.71 ± 0.03	–1.42
	E93A	8.03 ± 0.47	3.55 ± 0.03	–2.43
	E158A	7.57 ± 0.63	3.93 ± 0.04	0.27
	E159A	7.39 ± 0.45	3.99 ± 0.03	0.75

[a]Data were calculated from the GdnHCl-induced unfolding titration at each temperature fitted to a two-state Eq. 2. [b]Cooperativity in the two-state Eq. 1. [c]Mid-point of unfolding. [d]Difference in free-energy change between the wild type and the mutant, calculated using Eq. 3.

ble residue, Glu 158, which forms an intra-helical ion pair with Lys 161. The distances of these ion pairs are shown in Fig. 2. We constructed four mutants, E83A, E93A, E158A, and E159A.

Equilibrium Studies—To examine thermodynamic stability, GdnHCl-induced titration curves of the wild type and the mutants E83A, E93A, E158A, and E159A were obtained by measuring CD signals at 222 nm in the temperature range from 10°C to 70°C. Figure 3 shows a representative curve of the wild type at 20°C. Below 70°C *Tk*-MGMT shows full reversibility from its denaturant-unfolded form. The data obtained were well fitted to a conventional two-state equation (Eq. 1). The differences in free energy between the wild type and the mutants were calculated by Eq. 3. Table 1 lists the differences in unfolding free energies between the wild type and four mutants. At temperatures from 10°C to 70°C, the $\Delta\Delta G$ values of E83A, E93A, E158A, and E159A were –1.17 to –1.52 kJ mol^{-1}, –2.43 to –4.65 kJ mol^{-1}, 0.27 to 0.03, and –0.75 to 0.75 kJ mol^{-1}, respectively (Table 1, Fig. 4). The loss of free-energy change of E93A was larger than that of E83A, E158A, and E159A.

Table 2. **Melting temperatures of *Tk*-MGMT variants in 5 M urea[a].**

Proteins	T_m (°C)
wild type	91.5 ± 0.1
E83A	89.2 ± 0.1
E93A	85.5 ± 0.1
E158A	90.6 ± 0.2
E159A	91.7 ± 0.2

[a]Data were calculated from the temperature-induced unfolding curves monitored by CD at 222 nm.

Unfolding Kinetics—Figure 5 shows unfolding kinetics of *Tk*-MGMT variants at 50°C. The results of the unfolding kinetics of *Tk*-MGMT variants were complex. In general, unfolding, monitored by optical probes, follows a single-exponential curve because of the low stability of the intermediate under strongly denaturing conditions.

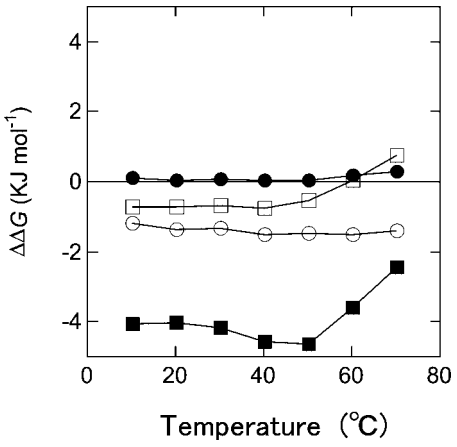

Fig. 4. **Temperature-dependent ΔΔ*G* profiles between the wild type and the mutants.** E83A, open circles; E93A, closed squares; E158A, closed circles; E159A, open squares.

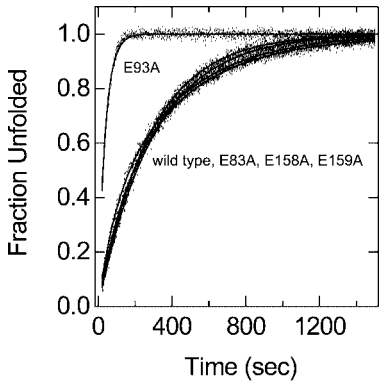

Fig. 5. **Kinetic traces of GdnHCl-induced unfolding transition monitored at CD 222 nm.** Time course of unfolding of *Tk*-MGMT variants at 7.84 M GdnHCl at 50°C. Solid lines show the results of the nonlinear regression analyses according to Eq. (4) with $i = 3$ for the wild type, $i = 3$ for E158A, $i = 2$ for E83A, $i = 2$ for E93A, $i = 3$ for E159A.

However, the unfolding process of the wild type between 10 and 500 s appeared to consist of three kinetic phases: 6.04×10^{-2} s^{-1} (~35% of the signal), 7.77×10^{-3} s^{-1} (~23% of the signal), and 1.31×10^{-3} s^{-1} (~42% of the signal). These three kinetic phases could be explained by the formation of the native structure from a fully unfolded state *via* two intermediate forms. The unfolding of mutants was also fitted to a multiple-exponential equation. The unfolding processes of E158A and E159A consisted of three kinetic phases, and those of E83A and E93A consisted of two phases. Most of the signal changes of the fastest phase observed in the wild type, E158A, and E159A occurred within the mixing dead time (10 s) and were discarded from our analysis. The rate constants of the middle and slowest phases were calculated from unfolding signals at 50°C. The unfolding rates of the middle phases of the wild type, E83A, E93A, E158A, and E159A were 7.77×10^{-3} s^{-1}, 2.36×10^{-2} s^{-1}, 2.83×10^{-2} s^{-1}, 1.31×10^{-2} s^{-1}, and 1.28×10^{-2} s^{-2}, respectively. The unfolding rate of the middle phase of the wild type was a little slower than that of the mutants, and no significant difference in rate constants among mutants could be detected. The unfolding rates of the slowest phases of the wild type, E83A, E93A, E158A, and E159A were 1.31×10^{-3} s^{-1}, 1.65×10^{-3} s^{-1}, 1.50×10^{-2} s^{-1}, 1.97×10^{-3} s^{-1}, 2.65×10^{-3} s^{-1}, respectively. The unfolding rate of the slowest phase of E93A was one order magnitude of faster than those of other variants (Fig. 5).

Melting Temperature of Tk-MGMT Variants in the Presence of 5 M Urea—The stability of *Tk*-MGMT variants was also evaluated by determining the melting temperature. This was done in the presence of 5 M urea, because *Tk*-MGMT variants were not denatured even at 100°C under the physiological conditions. The melting temperatures of the wild type, E83A, E93A, E158A, and E159A were 91.5°C, 89.2°C, 85.5°C, 90.6°C, and 91.7°C, respectively (Table 2). That of E93A was clearly lower than those of the wild type and other mutants. This result was consistent with the equilibrium study using GdnHCl. These results suggest that E93A was most destabilized among the four variants tested in this study.

Effects of Structural Change by Mutation on the Wild-Type Native Structure—To investigate the structural effects of mutation, measurements of far-UV CD spectra and computer simulation were performed. No differences in far-UV CD spectra were found between the wild type and mutants (data not shown). We also performed energy minimization for the *Tk*-MGMT variants using the computer program InsightII/DISCOVER. Calculated structures of the wild type and mutants are shown in Fig. 6. RMSDs of E83A, E93A, E158A, and E159A compared to the wild type were 0.679 Å, 1.088 Å, 0.720 Å, and 0.782 Å, respectively. These results suggest that the mutations did not cause large structural changes. Finally, we examined whether the mutations caused the formation of new ion pairs or hydrogen bonds, but in no case could such a change be predicted.

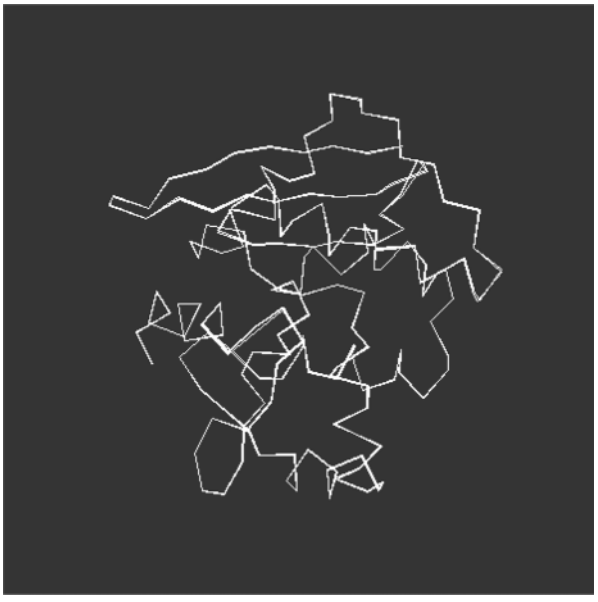

Fig. 6. **Superimposition of calculated structures of the wild type and mutants using energy minimization.**

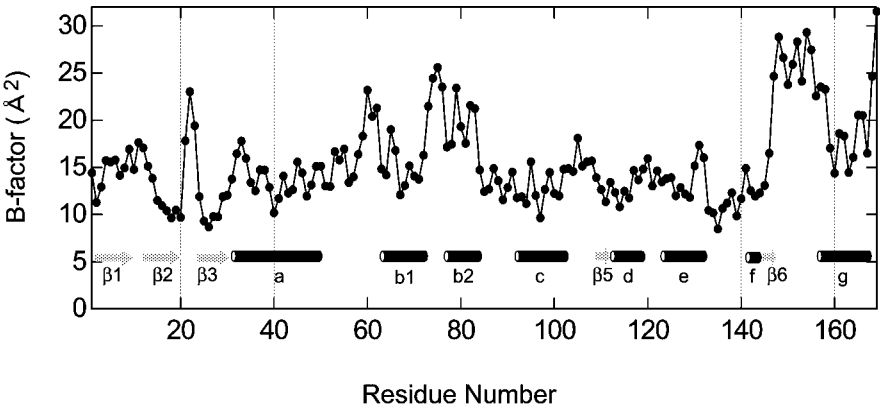

Fig. 7. **B-factor of Cα atoms versus the residue number.** Information on the secondary structure of *Tk*-MGMT is below the plot. β-sheets are shown as broad arrows and α-helices as barrels.

DISCUSSION

The objective of this study was to reconfirm the contribution of ion pairs to the thermodynamic and kinetic stability of a hyperthermophilic protein, *Tk*-MGMT. The stability of E158A, in which the intra-helical ion pair on the protein surface (Glu 158–Lys 161) was disrupted, exhibited almost the same value as the wild type. Of the three mutants with disrupted inter-helical ion pairs in the protein interior, E93A was the most destabilized, by ~4 kJ mol^{-1} for ΔG and by 6.0°C for T_m. In addition, the unfolding rate of E93A was one order of magnitude faster than those of the other variants. This result suggests that the disruption of the ion-pair network involving Glu 93 leads to the destabilization of the native structure of *Tk*-MGMT (~4 kJ mol^{-1}), which results in a lowering of the unfolding activation free-energy change. E83A was destabilized by ~1.5 kJ mol^{-1} for ΔG and by 2.3°C for T_m, while E159A was not destabilized. It is worth emphasizing that the SASA of Glu 93 (7.2%) is almost identical to that of Glu 159 (8.9%), whereas only E93A is destabilized in terms of both equilibrium and kinetics. These experimental data provide a new consideration regarding ion pairs, as follows.

There is no doubt about the role of single ion pairs on the protein surface. Many studies have shown that exposed ion-pair interactions contribute only marginally to the free-energy stabilization (*12–14*). It has been argued that the gain in electrostatic energy with the formation of ion pairs is offset by the entropic cost of desolvation and localization of the flexible side chain. In lines with this, our experiments showed that the ion pair involving Glu 158 does not contribute to protein stability. Similar observations have recently been made using a hyperthermophilic rubredoxin variant (*25*).

Internal ion pairs are more complex than those on the protein surface. In the interior of the protein, ion pairs undergo stronger electrostatic interactions than those on protein surface due to the lower dielectric environment (*18*, *26*). Some reports indicated that buried ion pairs contribute to protein stability (*9*, *10*). Takano *et al*. showed that the contribution of ion pairs in human lysozyme to protein stability correlated well with the SASA of ion pairs (*27*). On the other hand, buried ion pairs also pay a high desolvation penalty during folding. Kumar *et al*. calculated that average of desolvation penalty for 66 buried ion pairs was 54 kJ mol^{-1} (*18*). An experimental study suggested that buried ion pairs destabilized the folded protein (*28*). Therefore, it is difficult to predict the energy contribution of a buried ion pair to protein stability, because it is determined by a fine balance among the favorable electrostatic interactions, the unfavorable desolvation penalty, and the interaction of the ion pair with other residues.

In our study, the SASAs of Glu 93 and Glu 159 were almost the same, but E93A was clearly more destabilized than E159A. Although E93A had two disrupted inter-helical ion pairs, the normalized destabilization effect of E93A per ion pair was much larger than that of E159A. A study of mutagenesis in the NADP-binding domain of glutamate dehydrogenase derived from *Thermotoga maritima* indicated that an ion-pair interaction was strengthened by one of the partners being involved in a second ion-pair interaction (*29*). In that study, the interaction energy between Lys 193 and Glu 231 was 3.7 kJ mol^{-1} (estimated from the thermodynamic cycles), whereas this interaction destabilized the protein by 0.84 kJ mol^{-1} by the removal of the Arg 190 side chain. This phenomenon was also observed in molecular dynamics simulations on an ion-pair cluster of the DNA-binding protein Sac7d (*30*). In the theoretical study, each new member in a network of ion pairs requires the desolvation of just one residue (*31*), so that a network-forming ion pair is more favorable for protein stability than an isolated ion pair. In general, as the melting temperature of proteins increases, ion pairs tend to be organized into networks (*1*, *32*, *33*). This is an important issue when discussing the structural properties of E93A. Glu 93 formed an ion-pair network with Arg 50 and Arg 132, which occurred in the inter-helices between the a-helix and the c-helix and between the c-helix and the e-helix. This ion-pair network connects the N and C-terminal domains (Fig. 1B). Due to these structural features, this ion-pair network is thought to reinforce the internal packing of the tertiary structure and therefore contribute to the global stability.

Glu 83 also forms an ion-pair network with Lys 66, and Asp 62, which occurs in the inter-helix position between the b1- and b2-helices. However, E83A was less destabilized than E93A; in particular, the unfolding rate of E83A was almost identical to that of the wild type. The structural differences between Glu 83 and Glu 93 are (i) solvent accessibility and (ii) the pattern of network formation. (i) Glu 83 is partially exposed (16.9%), so this ion-pair network contributes less to protein stability than that involving Glu 93. (ii) The ion-pair network involving

Glu 83 connects adjacent helices (b1- and b2-helices) in the N-terminal domain, whereas that involving Glu 93 connects three helices and bridges the N- and C-terminal domains. Although Glu 83 is involved in an ion-pair network, E83A loses only one ion pair between Lys 66 and Glu 83. In a previous study, it was suggested that the inter-helical ion-pair between Lys and Glu contributed to the stability of the coiled-coil (*34*). A similar study demonstrated that inter-helical ion pairs stabilized the coiled-coil by 0.59–4.78 kJ mol^{-1} (*35*). These results suggest that inter-helical ion pairs are favorable for a tertiary structure. Glu 93 forms two inter-helical ion-pairs, while Glu 83 forms only one, as does Glu 159. Therefore, E93A might be most destabilized among the mutants tested in this study.

We also took into account the B-factor of the crystal structure, which relates to the fluctuations in the structure. The ion-pair network involving Glu 83 connects the b1-helix and the b2-helix, which showed relatively high B-factors, especially the b2-helix (Fig. 7). Therefore, the ion pair involving Glu 83 could not form a strong link between the b1- and b2-helices. Glu 159 forms an ion pair with Arg 39 between the a-helix and the g-helix (Fig. 1). In a previous study, the DNA-binding model of methyltransferase suggested that the g-helix is required to swivel by moving around the loop residues from β6 to the g-helix during catalysis (*36*). Indeed, the B-factor of the loop between β6 and the g-helix was very high (Fig. 7), implying that this region is not so important in stabilizing the global structure of *Tk*-MGMT.

Hyperthermophilic proteins tend to have a large number of ion-pairs on the protein surface (*37*). It has been reported that optimizing the charge-charge interactions on the protein surface contributes to protein stability (*38*) and that proteins in general gain electrostatic stabilization by minimizing the number of repulsive contacts (*39*). Electrostatic interactions on the protein surface may contribute to protein stability, not by forming a single ion pair, but by organizing the global electrostatics. The SASAs values of charged side-chains are thought to be one of the criteria necessary for predicting the energy contribution of ion pairs. However, we found no clear relationship between the accessible surface area and the energy contribution to protein stability, indicating the importance of the structural features and formation patterns of ion pairs.

In conclusion, ion pairs can contribute to the stability of *Tk*-MGMT when they exist in certain locations: (i) in the interior, (ii) in an inter-helix or inter-domain, (iii) in an ion-pair network and (iv) in regions with low values of the B-factor. In these locations, ion pairs stabilize the internal packing of the tertiary structure, in cooperation with a hydrophobic interaction to connect between the helices and the domains. These features, along with the simple accessibility of the side-chain, may be keys to understanding the thermodynamic and thermal stability of hyperthermophilic proteins. In the future, a crystallographic study of the mutants shoud help us to understand the effects of ion pairs more precisely.

This work was supported by a Grant-in-Aid for Scientific Research from the Ministry of Education, Science, Sports and Culture of Japan (14350433, 14045229) and a grant from the Science and Technology Incubation Program in Advanced Region by Japan Science and Technology Corporation (JST). We thank Dr. Judith Steeh, head editor, Technical Communication Program in Japan Advanced Institute of Science and Technology, for helpful comments and critical reading of the manuscript. This work was partly supported by a 21st century COE program called "Scientific Knowledge Creation Based on Knowledge Science" by Japan Advanced Institute of Science and Technology.

REFERENCES

1. Yip, K.S.P., Stillman, T.J., Britton, K.L., Artymiuk, P.J., Baker, P.J., Sedelniova, S.E., Engel, P.C., Pasquo, A., Chiaraluce, R., Consalvi. V, Scandurra, R., and Rice, D.W. (1995) The structure of *Pyrococcus furiosus* glutamate dehydrogenase reveals a key role for ion-pair networks in maintaining enzyme stability at extreme temperature. *Structure* **3**, 1147–1158
2. Day, M.W., Hsu, B.T., Joshua-tor, L., Park, J.B., Zhou, Z.H., Adams, M.W.W., and Rees, D. (1992) X-ray crystal structures of the oxidized and reduced forms of the rubredoxin from the marine hyperthermophilic archaebacterium *Pyrococcus furiosus*. *Protein Sci.* **1**, 1494–1507
3. Korndofer, I., Steipe, B., Huber, R., Tomschy, A., and Jaenicke, R. (1995) The crystal structure of holo-glyceraldehyde-3-phosphate dehydrogenase from the hyperthermophile bacterium *Thermotoga maritima*. *J. Mol. Biol.* **246**, 511–521
4. Hennig, M., Darimont, B., Stermer, R., Kirschner, K., and Jansonius, J.N. (1995) 2.0 Å structure of indole-3-glycerol phosphate synthase from the hyperthermophile *Sulfolobus solfataricus*: possible determinants of protein stability. *Structure* **3**, 1295–1306
5. Lim, J., Yu, Y.G., Han, Y.S., Cho, S., Ahn, B., Kim, S., and Cho, Y. (1997) The crystal structure of an Fe-superoxide dismutase from the hyperthermophile *Aquifex pyrophilus* at 1.9 Å resolution: structural basis for thermostability. *J. Mol. Biol.* **270**, 259–274
6. Xu, D., Lin, S.L., and Nussinov, R. (1997) Protein binding versus protein folding: the role of hydrophilic bridges in protein associations. *J. Mol. Biol.* **265**,68–84
7. Horovitz, A. and Fersht, A.R. (1992) Co-operative interactions during protein folding. *J. Mol. Biol.* **224**, 733–740
8. Marqusee, S. and Sauer, R.T. (1994) Contribution of a hydrogen bond/salt bridge network to the stability of secondary and tertiary structures in lambda repressor. *Protein Sci.* **3**, 2217–2225
9. Pervushin, K., Billeter, M., Siegal, G., and Wuthrich, K. (1996) Structural role of buried salt bridge in the 434 repressor DNA-binding domain. *J. Mol. Biol.* **264**, 1002–1012
10. Tissot, A.C., Vuilleumier, S., and Rersht, A.R. (1996) Importance of two buried salt bridges in the stability and folding pathway of barnase. *Biochemistry* **35**, 6786–6794
11. Lounnas, V. and Wade, R.C. (1997) Exceptionally stable salt bridges in cytochrome P450cam have functional roles. *Biochemistry* **36**, 5402–5417
12. Singh, U.C. (1988) Probing the salt bridge in the dihydrofolate reductasemethotrexate complex by using the coordinate-coupled free energy perturbation method. *Proc. Natl. Acad. Sci. USA* **85**, 4280–4284
13. Serrano, L., Horovitz, A., Avron, B., Bycroft, M., and Fersht, A.R. (1990) Estimating the contribution of engineered surface electrostatic interactions to protein stability by using double mutant cycles. *Biochemistry* **29**, 9343–9352
14. Barril, X., Aleman, C., Orozco, M., and Luque, F.J. (1998) Salt bridge Interactions: stability of ionic and neutral complexes in the gas phase, in solution and in proteins. *Proteins* **32**, 67–79
15. Sunn, D.P., Sauer, U., Nicholson, H., and Matthews, B.W. (1991) Contributions of engineered surface salt bridges to the stability of T4 lysozyme determined by directed mutagenesis. *Biochemistry* **30**, 7142–7153

16. Dao-pin, S., Anderson, D.E., Baase, W.A., Dahlquit, F.W, and Matthews, B.W. (1991) Structural and thermodynamic consequences of burying a charged residue within the hydrophobic core of T4 lysozyme. *Biochemistry* **30**, 11521–11529
17. Hendsch, Z.S. and Tidor, B. (1994) Do salt bridges stabilize protein? A continuum electrostatic analysis. *Protein Sci.* **3**, 211–22
18. Kumar, S. and Nussinov, R. (1999) Salt bridge stability in monomeric proteins. *J. Mol. Biol.* **293**, 1241–1255
19. Shiraki, K., Nishikori, S., Fujiwara, S., Hashimoto, H., Kai, Y., Takagi, M., and Imanaka, T. (2001) Comparative analyses of the conformational stability between a hyperthermophilic protein and its mesophilic counterpart. *Eur. J. Biochem.* **268**, 4144–4150
20. Hashimoto, H., Inoue, T., Nishioka, M., Fujiwara, S., Takagi, M., Imanaka, T., and Kai, Y. (1999) Hyperthermostable protein structure maintained by intra- and inter- helix ion-pairs in archaeal O^6-methylguanine-DNA methyltransferase. *J. Mol. Biol.* **292**, 707–716
21. Marqsee, S. and Baldwin, R.L. (1987) Helix stabilization by Glu^-–Lys^+ salt bridges in short peptides of de novo design. *Proc. Natl. Acad. Sci. USA* **84**, 8898–8902
22. Leclere, M.M., Nishioka, M., Yasuda, T., Fujiwara, S., Takagi, M., and Imanaka, T. (1998) The O^6-methylguanine-DNA methyltransferase from the hyperthermophilic archaeon *Pyrococcus* sp. KOD1: a thermostable repair enzyme. *Mol. Gen. Genet.* **258**, 69–77
23. Gill, S.C. and von Hippel, P.H. (1989) Calculation of protein extinction coefficients from amino acid sequence data. *Anal. Biochem.* **182**, 319–326
24. Horovitz, A. (1996) Double-mutant cycles: a powerful tool for analyzing protein structure and function. *Fold. Des.* **1**, 121–126
25. Strop, P. and Mayo, S.L. (2000) Contribution of surface salt bridges to protein stability. *Biochemistry* **39**, 1251–1255
26. Basie, C.A. and Berg, J.M. (1997) Electrostatic interactions across a beta-sheet. *Biochemistry* **36**, 6218–6222
27. Takano, K., Tsuchimori, K., Yamagata, Y., and Yutani, K. (2000) Contribution of salt bridges near the surface of a protein to the conformational stability. *Biochemistry* **39**, 12375–12381
28. Waldburger, C.D., Schidbach, J.F., and Sauer, R.T. (1995) Are buried salt bridges important for protein stability ad conformational specificity? *Nat. Struct. Biol.* **2**, 122–128
29. Lebbink, J.H.G., Consalvi, V., Chiaraluce, R., Berndt, K.D., and Ladenstein, R. (2002) Structural and thermodynamic studies on a salt-bridge triad in the NADP-binding domain of glutamate dehyderogenase from *Thermotoga maritima*: Cooperativity and electrostatic contribution to stability. *Biochemistry* **41**, 15524–15535
30. de Bakker, P.I., Hunenberger, P.H., and McCammon, J.A. (1999) Molecular dynamics simulations of the hyperthermophilic protein sac7d from *Sulfolobus acidocaldarius*: contribution of salt bridges to thermostability. *J. Mol. Biol.* **285**, 1811–1830
31. Yip, K.S., Britton, K.L., Stillman, T.J., Lebbink, J., de Vos, W.M., Robb, F.T., Vetriani, C., Maeder, D., and Rice, D.W. (1998) Insights into the molecular basis of thermal stability from the analysis of ion-pair networks in the glutamate dehydrogenase family. *Eur. J. Biochem.* **255**, 336–346
32. Russell, R.J.M., Gerike, U., Danson, M.J., Hohgh, D.W., and Taylor, G.L. (1998) Structural adaptations of the cold-active citrate synthase from an Antarctic bacterium. *Structure* **6**, 351–361
33. Kim, S.Y., Hwang, K.Y., Kim, S.H., Sung, H.C., Han, Y.S., and Cho, Y. (1999) Structural basis for cold adaptation. *J. Biol. Chem.* **274**, 11761–11767
34. Zhou, N.E., Kay, C.M., and Hodges, R.S. (1994) The role of energetic contribution of interhelical electrostatic attractions to coiled-coil stability. *Protein Eng.* **7**, 1365–1372
35. Krylov, D., Mikhailenko, I., and Vinson, C. (1994) A thermodynamic scale for leucine zipper stability and dimerization specificity: e and g interhelical interactions. *EMBO J.* **13**, 2849–2861
36. Moore, M.H., Gulbism, J.M., Dodson. E, J, , Demple. B., and Moody, P.C. (1994) Crystal structure of a suicidal DNA repair protein: the Ada O^6-methylguanine-DNA methyltransferase from *E. coli*. *EMBO J.* **13**, 1495–1501
37. Goldman, A. (1995) How to make my blood boil. *Structure* **15**, 1277–1279
38. Loladze, V.V., Ibarra-Molero, B., Sanchez-Ruiz, J.M., and Makhatadze, G.I. (1999) Engineering a thermostable protein *via* optimization of charge-charge interactions on the protein surface. *Biochemistry* **38**, 16149–16423
39. Spassov, V.Z., Ladenstein, R., and Karshikoff, A.D. (1994) Optimization of the electrostatic interactions between ionized groups and peptide dipoles in proteins. *Protein Sci.* **4**, 1516–1527